Available online at www.sciencedirect.com
SCIENCE DIRECT®
Journal of Sound and Vibration 273 (2004) 857–874
JOURNAL OF SOUND AND VIBRATION
www.elsevier.com/locate/jsvi

Effect of non-linearity in free large oscillations of a shallow catenary

C.B. Rawlins*

16 Riverside Parkway, Massena, NY 13662, USA

Received 11 November 2002; accepted 12 May 2003

Abstract

Non-linear effects in free large amplitude oscillations of a shallow catenary are analyzed by representing the motion in terms of the well-known linear eigenmodes. The motion is comprised of a fundamental frequency and its harmonics. For each harmonic, including the fundamental, the mode shape is synthesized from the linear eigenmodes. The equation of motion is then cast as a non-linear eigenproblem to determine the fundamental frequency and the amplitudes of the contributory linear eigenmodes at each harmonic. Numerical results confirm the previously reported shift of the fundamental frequency due to non-linear effects as amplitude increases. The shift is found to have both tension- and non-tension-dependent components. For given structural assumptions, there may be different solutions to the non-linear equation of motion, differing significantly in mode shape and waveform.

1. Introduction

Galloping is a low-frequency wind-induced vibration of overhead electrical lines caused by aeroelastic instability when the cables become coated with ice. The motion is predominantly in the vertical plane. In most cases, the galloping encompasses a series of spans which interact through swinging of suspension insulators at supporting towers, but it also occurs in single ''deadended'' spans supported rigidly at both ends.

The vibration takes the form approximately of free eigenmodes of the single span or of the multispan section, that is, those that exist in the absence of wind and damping. These modes have been determined from the linearized equations of motion [1–4]. However, the conditions that attend actual galloping can sometimes exceed the range where non-linear effects can be ignored.

*Tel.: +1-315-764-0817; fax: +1-315-769-6740.
E-mail address: rawlins@ieee.org (C.B. Rawlins).

0022-460X/$ - see front matter © 2003 Elsevier Ltd. All rights reserved.
doi:10.1016/S0022-460X(03)00646-1

There are several sources of non-linearity in natural galloping. One is the fact that the aerodynamic coefficients involved in galloping are functions of angle of attack within the range encountered in the field. This area has been explored extensively, beginning with Den Hartog's pioneering paper in 1932 [5]. A recent contribution is that of Yu et al. [6]. Another source is kinematic. The effective longitudinal stiffness of suspension insulator supports increases as the longitudinal displacement increases, an area currently under investigation by Havard [7].

A third source of non-linearity, and the subject of this paper, is the modulation of cable tension by the galloping motion. This modulation is inherent to certain of the modes of oscillation that are found in natural galloping quite independent of aerodynamic and kinematic effects. Its effects are difficult to analyze. They are most accessible through study of the free oscillation of a single rigidly supported span. Although the term "galloping" applies strictly only to wind excited motions, it is for convenience applied in what follows to the free oscillations under study here.

This problem has been addressed previously. The single-span case has been analyzed by Hagedorn and Schäfer [8] and Luongo et al. [9], and Rienstra has dealt with both single and multispan cases [10]. Perturbation methods were employed.

This paper describes an approach to the free oscillation problem in which the non-linear behavior is cast as a non-linear eigenproblem. An eigenvalue approach is suggested by the finding of previous investigators that the frequency of galloping becomes unknown when non-linear effects are introduced. The approach makes it feasible to represent the motion by a linear combination of eigenmodes, in this case the eigenmodes of the linear problem. High accuracy is possible by including many modes in the sum. The analysis focuses on the single-span case, and addresses only the symmetric modes, those having odd numbers of loops in the span, since non-linear effects are most significant there.

In the approach described here, motion of the span takes place at a certain fundamental circular frequency ω_g and its harmonics $r\omega_g$ ($r = 1, 2, 3, \ldots$). At each harmonic, the shape of the cable is a combination of the eigenmodes of the linearized problem. Non-linear effects couple the various eigenmodes at the various harmonics to one another. These couplings are expressed in terms of the generalized forces, generalized masses and frequency offsets involved. The couplings are assembled in a non-linear stiffness matrix which, together with the corresponding matrices for the linear problem, form the non-linear equation of motion.

2. Analysis

Analysis is simplified by choosing the co-ordinate system shown in Fig. 1. The catenary is assumed to be shallow enough that it can be approximated by a circular arc of curvature σ, and

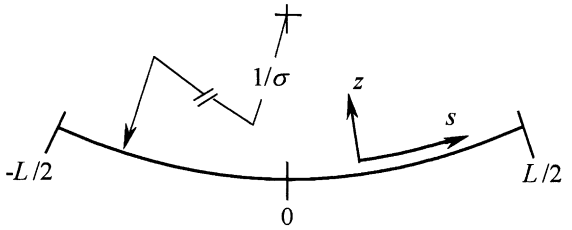

Fig. 1. Co-ordinate system.

the component of gravity normal to the arc is assumed to be essentially the same as gravity itself. Let the cable tension be T, its mass μ, and the instantaneous displacement of the cable be $z(s,t) = y(s)\cos\omega t$. With these assumptions, the equation of motion becomes [4]

$$-\mu g - \mu\frac{\partial^2 z}{\partial t^2} + \frac{\partial}{\partial s}\left(T\frac{\partial z}{\partial s}\right) + T\sigma = 0. \tag{1}$$

Let the tension be comprised of constant and variable components: $T = T_g + \zeta$, where $\zeta(s,t) = \tau(s)\cos\omega t$. This leads to

$$-\mu g - \mu\frac{\partial^2 z}{\partial t^2} + \frac{\partial}{\partial s}\left[(T_g + \zeta)\frac{\partial z}{\partial s}\right] + (T_g + \zeta)\sigma = 0. \tag{2}$$

The weight of the cable μg is supported by the tension curvature product $T_g\sigma$, so those terms cancel. Now, in practical spans, tension waves travel at about 50 times the speed of transverse waves. Thus, although ζ varies sinusoidally with time, it can be taken as constant over the span. Then, $\partial\zeta/\partial s = 0$, and the equation of motion becomes

$$-\mu\frac{\partial^2 z}{\partial t^2} + T_g\frac{\partial^2 z}{\partial s^2} + \zeta\frac{\partial^2 z}{\partial s^2} + \zeta\sigma = 0. \tag{3}$$

The third term is the source of non-linearity since both ζ and z are variables. However, since it is of second order, the term can be neglected when motion is small. What remains is the linearized equation of motion.

2.1. Linear eigenmodes

Solutions to the linear problem take the form [2]

$$y = u\left(\cos\lambda\frac{s}{L} - \cos\frac{\lambda}{2}\right), \tag{4}$$

where λ is a root of

$$\tan\frac{\lambda}{2} = \frac{\lambda}{2}\left(1 - \frac{\lambda^2}{\delta}\right) \tag{5}$$

with

$$\delta = \frac{\sigma^2 L^2 EA}{T}, \quad \lambda = \frac{\omega L}{c}, \quad c = \sqrt{\frac{T}{\mu}}, \tag{6}$$

δ being the catenary elasticity parameter, small values corresponding generally to shallow sags and large values to deep sags. If the excess of arc length of the span over secant span length is expressed as strain ε_c, and the elastic strain due to T is ε_0, then $\delta = \varepsilon_c/24\varepsilon_0$.

For every value of δ, Eq. (5) yields an infinite series of values for the frequency parameter λ. The first four of these eigenvalues are shown in Fig. 2. Each λ determines an eigenmode via Eq. (4). The eigenmodes for each δ are orthogonal.

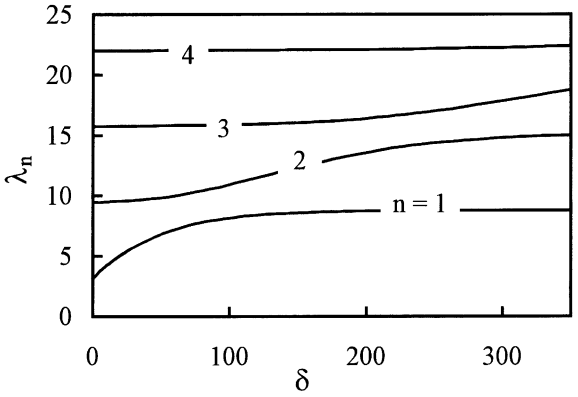

Fig. 2. Linear solution eigenvalues.

2.2. Assumed solution for non-linear problem

If oscillation takes place at circular frequency ω_g, variations in both z and ζ will occur at that frequency. When the variations are large enough that the non-linear third term in Eq. (3) becomes significant, that term will contain the product $\cos\omega_g t\cos\omega_g t = \frac{1}{2}(1+\cos 2\omega_g t)$. Thus, that term contributes a steady force to the equation of motion, as well as one at frequency $2\omega_g$. To the extent that the cable responds to the force at $2\omega_g$, additional elements will be appended to the non-linear term involving $\cos\omega_g t\cos 2\omega_g t$ and $\cos 2\omega_g t\cos 2\omega_g t$, and resulting in forces at ω_g, $3\omega_g$ and $4\omega_g$. Cable response to those forces will generate more harmonics of ω_g, evidently without limit. It is apparent that the cable's motion may be considered to have components at ω_g and all of its harmonics.

The (non-linear) mode shape and amplitude for each harmonic need to be determined. Since the linear eigenmodes are orthogonal, any non-linear mode shape can be synthesized from some combination of them. Therefore, a solution is assumed of the form

$$z = \sum_{r=1}^{\infty}\sum_{n=1}^{\infty} u_{r,n}\left(\cos\lambda_n\frac{s}{L} - \cos\frac{\lambda_n}{2}\right)\cos r\omega_g t. \tag{7}$$

This representation is similar to that of Rienstra [10], who used $n\lambda_1$ to generate the component mode shapes from Eq. (5), rather than the λ_n roots of Eq. (5). Solution (7) may be represented as a vector of amplitudes:

$$\langle u_{r,n}\rangle = \left[u_{1,1}u_{1,2}u_{1,3}\ldots u_{2,1}u_{2,2}u_{2,3}\ldots u_{3,1}u_{3,2}u_{3,3}\ldots\right]^{\mathrm{T}}. \tag{8}$$

However, it is not feasible in practice to deal with doubly infinite vectors, so in what follows it should be understood that the above summations are carried only to some upper index h, and the notation

$$u_{(r-1)\cdot h+n} = u_{r,n} \tag{9}$$

is adopted.

It will be convenient to normalize u against the sag of the catenary. Normalized amplitudes are defined by

$$U_{r,n} = \frac{u_{r,n}}{D_g}. \tag{10}$$

For shallow catenaries,

$$D \approx \sigma L^2/8. \tag{11}$$

Note that, among other things, non-linear effects induce changes in static tension T and sag D. At-rest conditions are distinguished by subscript c (calm) and those during galloping by the subscript g. Thus, definition (10) employs the sag as modified by non-linear effects.

2.3. Dynamic tensions

Tension variations τ are caused by variations in the arc length of the cable as it is distorted by the assumed eigenmodes. These variations have linear and non-linear components, $\varepsilon 1$ and $\varepsilon 2$ respectively. The linear component is associated with the interaction of displacement y with the catenary curvature σ. It can be demonstrated from Fig. 1 that the average strain of the cable due directly to amplitude $y(s)$ is

$$\varepsilon 1(s) = -\frac{1}{L}\int_{-L/2}^{L/2} \sigma y(s)\,\mathrm{d}s. \tag{12}$$

Using Eq. (4), the strain from linear eigenmode n at harmonic r is

$$\varepsilon 1_{r,n} = -\frac{\sigma}{L}\int_{-L/2}^{L/2} u_{r,n}\left(\cos\lambda_n\frac{s}{L} - \cos\frac{\lambda_n}{2}\right)\mathrm{d}s = -\sigma u_{r,n}\left(\frac{2}{\lambda_n}\sin\frac{\lambda_n}{2} - \cos\frac{\lambda_n}{2}\right). \tag{13}$$

Then from Eqs. (5), (6), (10) and (11) one obtains

$$\varepsilon 1_{r,n} = \frac{\sigma}{\delta}u_{r,n}\lambda_n^2\cos\frac{\lambda_n}{2} = \frac{\sigma D_g}{\delta}U_{r,n}\lambda_n^2\cos\frac{\lambda_n}{2} = \frac{1}{8}\frac{T_g}{EA}U_{r,n}\lambda_n^2\cos\frac{\lambda_n}{2}. \tag{14}$$

The total strain at harmonic r is

$$\varepsilon 1_r = \frac{1}{8}\frac{T_g}{EA}\sum_{n=1}^{h} U_{r,n}\lambda_n^2\cos\frac{\lambda_n}{2}. \tag{15}$$

Defining the static component of strain as

$$\varepsilon_0 = T_g/EA \tag{16}$$

results in

$$\varepsilon 1_r = \frac{\varepsilon_0}{8}\sum_{n=1}^{h} U_{r,n}\lambda_n^2\cos\frac{\lambda_n}{2}. \tag{17}$$

The non-linear component of cable strain is associated with its slope with respect to the catenary and corresponds to the strain of the deflected shape in vibration of a taut string. This strain is given by

$$\varepsilon 2(s,t) = \sqrt{1 + \left(\frac{\mathrm{d}z}{\mathrm{d}s}\right)^2} - 1 \approx \frac{1}{2}\left(\frac{\mathrm{d}z}{\mathrm{d}s}\right)^2. \tag{18}$$

Using Eq. (7), the average of this strain over the span due to motion at harmonic q becomes

$$\varepsilon 2_q(t) = \cos^2 q\omega_g t \frac{1}{2L}\int_{-L/2}^{L/2}\left(\sum_{n=1}^{\infty} u_{q,n}\frac{\lambda_n}{L}\sin\lambda_n\frac{s}{L}\right)^2 \mathrm{d}s \tag{19}$$

$$= \cos^2 q\omega_g t \sum_{n=1}^{\infty} u_{q,n}^2 \frac{\lambda_n^2}{4L^2}\left(1-\frac{\sin\lambda_n}{\lambda_n}\right). \tag{20}$$

Then from Eqs. (10), (11), (16) and (6),

$$\varepsilon 2_q(t) = \frac{\delta}{512}\varepsilon_0(1-\cos 2q\omega_g t)\sum_{n=1}^{\infty} U_{q,n}^2\lambda_n^2\left(1-\frac{\sin\lambda_n}{\lambda_n}\right).$$

Thus, there is a steady component of strain

$$\varepsilon 2_s = \frac{\delta}{512}\varepsilon_0\sum_{q=1}^{\infty}\sum_{n=1}^{\infty} U_{q,n}^2\lambda_n^2\left(1-\frac{\sin\lambda_n}{\lambda_n}\right), \tag{21}$$

and a dynamic component

$$\varepsilon 2_q = \cos 2q\omega_g t\frac{\delta}{512}\varepsilon_0\sum_{n=1}^{\infty} U_{q,n}^2\lambda_n^2\left(1-\frac{\sin\lambda_n}{\lambda_n}\right), \tag{22}$$

which exists only at even harmonics of the galloping frequency. The total dynamic strain at harmonic r is

$$\varepsilon_r = \varepsilon 1_r + \varepsilon 2_{r/2}, \tag{23}$$

with $r/2$ confined to integer values. The associated tension variation is

$$\zeta_p = \tau_p \cos p\omega_g t = EA\varepsilon_p. \tag{24}$$

2.4. Distributed force due to non-linear term

The force in Eq. (3) due to non-linearity arises from the interaction of dynamic tension variations with dynamic curvature of the cable. Those variations and curvatures are assumed to exist at all harmonics of ω_g up to some level h. It will now be necessary to keep track of the various harmonics of these several variables. To do that, let p be the harmonic of ω_g associated with tension variation, q the harmonic of ω_g associated with curvature variation, and r the harmonic of ω_g associated with the resulting force.

The interactions take the form $\tau_p \cos p\omega_g t \cdot y_q'' \cos q\omega_g t$, in which, from Eqs. (4), (10) and (11),

$$y_q'' = \sum_{n=1}^{h} y_{q,n}'' = -\sum_{n=1}^{h} u_{q,n}\frac{\lambda_n^2}{L^2}\cos\lambda_n\frac{s}{L} = -\frac{\sigma}{8}\sum_{n=1}^{h} U_{q,n}\lambda_n^2\cos\lambda_n\frac{s}{L}. \tag{25}$$

y''_q is the net dynamic curvature at harmonic q from all the linear eigenmodes. Then the distributed force from τ_p and y''_q can be written as

$$P_r(s,t) = -\cos p\omega_g t \cos q\omega_g t \frac{\sigma EA}{8} \varepsilon_p \sum_{n=1}^{h} U_{q,n}\lambda_n^2 \cos \lambda \frac{s}{L}. \tag{26}$$

2.5. Generalized forces

The generalized force from harmonic r on mode m is defined as

$$F_{r,m} = \int_{-L/2}^{L/2} P_r(s,t)\varphi_m(s)\,\mathrm{d}s, \tag{27}$$

where the mode shape for mode m, from Eq. (4), is

$$\varphi_m(s) = \cos \lambda_m \frac{s}{L} - \cos\frac{\lambda_m}{2}. \tag{28}$$

Thus,

$$\begin{aligned} F_{r,m} &= -\cos p\omega_g t \cos q\omega_g t \frac{\sigma EA}{8} \varepsilon_p \sum_{n=1}^{h} \left[U_{q,n} \int_{-L/2}^{L/2} \lambda_n^2 \cos\frac{\lambda_n s}{L}\left(\cos\frac{\lambda_m s}{L} - \cos\frac{\lambda_m}{2}\right) \mathrm{d}s \right] \\ &= -\cos p\omega_g t \cos q\omega_g t \frac{\sigma EAL}{8} \varepsilon_p \sum_{n=1}^{h} U_{q,n}\lambda_m\lambda_n \left[\frac{\sin(\lambda_m-\lambda_n)/2}{\lambda_m-\lambda_n} - \frac{\sin(\lambda_m+\lambda_n)/2}{\lambda_m+\lambda_n} \right]. \end{aligned} \tag{29}$$

Define

$$H_{m,n} = \lambda_m\lambda_n \frac{\sin(\lambda_m-\lambda_n)/2}{\lambda_m-\lambda_n} - \frac{\sin(\lambda_m+\lambda_n)/2}{\lambda_m+\lambda_n}. \tag{30}$$

Then, using Eqs. (16) and (30), one has

$$F_{r,m} = -\cos p\omega_g t \cos q\omega_g t \frac{\sigma T_g L}{8} \frac{\varepsilon_p}{\varepsilon_0} \sum_{n=1}^{h} U_{q,n} H_{m,n}. \tag{31}$$

2.6. Inter-harmonic couplings

Regarding Eq. (31), note that

$$\cos p\omega_g t \cos q\omega_g t = \frac{\cos(p-q)\omega_g t + \cos(p+q)\omega_g t}{2}. \tag{32}$$

Thus, generalized forces at harmonic r can result from only certain combinations of p and q, described by $r = p - q$ and $r = p + q$. Since $\cos(x) = \cos(-x)$, the first of these can be written as $r = |p - q|$. The two relations can be rewritten as $p = |r - q|$ and $p = r + q$. Then, summing over all the combinations of p and q that can produce harmonic r, Eq. (31) becomes

$$F_{r,m} = -\frac{\sigma T_g L}{8} \cos r\omega_g t \sum_{q=1}^{h} \left[G_{r,q} \sum_{n=1}^{h} \left(U_{q,n} \cdot H_{m,n} \right) \right], \tag{33}$$

in which

$$G_{r,q} = \frac{\varepsilon_{|r-q|} + \varepsilon_{r+q}}{2\varepsilon_0}. \tag{34}$$

2.7. Static force due to non-linearity

Non-linear effects influence the static position of the catenary. First, when dynamic tension and dynamic curvature are at the same harmonic, so that $p = q$, Eq. (26) becomes

$$P_r(s,t) = -\frac{1+\cos 2q\omega_g t}{2}\frac{\sigma EA}{8}\varepsilon_q \sum_{n=1}^{h} U_{q,n}\lambda_n^2 \cos\lambda\frac{s}{L}. \tag{35}$$

The effect of the time-dependent part here is covered in Eq. (33). There remains a static force from each harmonic:

$$S_q(s) = -\frac{\sigma EA}{16}\varepsilon_q \sum_{n=1}^{h} U_{q,n}\lambda_n^2 \cos\lambda\frac{s}{L}. \tag{36}$$

The total from all harmonics is

$$S(s) = -\frac{\sigma EA}{16}\sum_{q=1}^{h}\varepsilon_q \sum_{n=1}^{h} U_{q,n}\lambda_n^2 \cos\lambda\frac{s}{L}. \tag{37}$$

This force distorts the catenary in two ways. First, its average $\bar{S}$ over the span augments the $T_g\sigma$ term in Eq. (2):

$$\bar{S} = -\frac{\sigma EA}{16}\sum_{q=1}^{h}\varepsilon_q \sum_{n=1}^{h} U_{q,n}\lambda_n^2 \frac{1}{L}\int_{-L/2}^{L/2}\cos\lambda_n\frac{s}{L}\,\mathrm{d}s = -\frac{\sigma EA}{8}\sum_{q=1}^{h}\varepsilon_q \sum_{n=1}^{h} U_{q,n}\lambda_n \sin\frac{\lambda_n}{2}. \tag{38}$$

It is an internal force, like $T_g\sigma$, so it shares in supporting the cable weight μg.

The second component of static force arises from $\varepsilon 2_s$ (see Eq. (21)). This causes an increment in tension

$$\tau 2 = EA\varepsilon 2_s. \tag{39}$$

That increment applies upward pressure on the catenary in the amount $\sigma\tau 2$.

The sum of $\bar{S}$ and $\sigma\tau 2$ accounts for the difference between T_g and T_c referred to earlier. Its effect upon tension, sag and average curvature σ is the same as obtained by applying $\bar{S} + \sigma\tau 2$ as a negative increment to μg. The change in tension $\Delta T/T_g$ may be found as a root of

$$\left(1+\frac{\Delta T}{T_g}\right)^2\left(1+\frac{24}{\delta}\frac{\Delta T}{T_g}\right) - \left(1-\frac{\bar{S}+\sigma\tau 2}{\mu g - \bar{S} - \sigma\tau 2}\right) = 0. \tag{40}$$

Note that ΔT is the change from T_c to T_g. The various relations above can only be evaluated when the eigenvalues λ_n during galloping are known. Thus, δ, on which they depend, and therefore T in Eq. (6) must be those that exist during galloping. This is somewhat inconvenient, since it is usually the at-rest value T_c that is directly available. This necessitates assuming several trial values of T_g to discover the one that leads back to T_c via $T_c = T_g - \Delta T$.

The change in average curvature $\Delta\sigma$ can be calculated from

$$\bar{S} = \Delta(\sigma T) = (\sigma_g + \Delta\sigma)(T_g + \Delta T) - \sigma_g T_g. \tag{41}$$

Then $\sigma_c = \sigma_g - \Delta\sigma$. At rest and during galloping, sags can be calculated from σ_c and σ_g.

Static force $S(s)$ also distorts the catenary locally, making it meander about the arc defined by σ_g. The deviations in curvature due to this meandering interact with the dynamic tension components τ_r to produce dynamic forces at frequency $r\omega_g$. The deviation in static curvature is given by

$$\frac{S(s) - \bar{S}}{T_g} = -\frac{\sigma EA}{16T_g}\sum_{q=1}^{h}\varepsilon_q \sum_{n=1}^{h} U_{q,n}\lambda_n^2\left(\cos\lambda_n\frac{s}{L} - \frac{2}{\lambda_n}\sin\frac{\lambda_n}{2}\right). \tag{42}$$

The resulting force distribution at harmonic r is

$$-EA\varepsilon_r\frac{\sigma EA}{16T_g}\sum_{q=1}^{h}\varepsilon_q \sum_{n=1}^{h} U_{q,n}\lambda_n^2\left(\cos\lambda_n\frac{s}{L} - \frac{2}{\lambda_n}\sin\frac{\lambda_n}{2}\right). \tag{43}$$

It is applied at each of the eigenmodes m in accordance with Eq. (27), resulting in the generalized force

$$N_{r,m} = -\varepsilon_r\frac{\sigma(EA)^2}{16T_g}\sum_{q=1}^{h}\varepsilon_q \sum_{n=1}^{h} U_{q,n}\lambda_n^2\int_{-L/2}^{L/2}\left(\cos\lambda_n\frac{s}{L} - \frac{2}{\lambda_n}\sin\frac{\lambda_n}{2}\right)\left(\cos\lambda_m\frac{s}{L} - \cos\frac{\lambda_m}{2}\right)\mathrm{d}s. \tag{44}$$

The integral reduces to

$$L\left[\frac{\sin(\lambda_m - \lambda_n)/2}{\lambda_m - \lambda_n} + \frac{\sin(\lambda_m + \lambda_n)/2}{\lambda_m + \lambda_n} - \frac{4}{\lambda_m\lambda_n}\sin\frac{\lambda_m}{2}\sin\frac{\lambda_n}{2}\right]. \tag{45}$$

Define

$$J_{m,n} = \frac{\lambda_n^2}{2}\left[\frac{\sin(\lambda_m - \lambda_n)/2}{\lambda_m - \lambda_n} + \frac{\sin(\lambda_m + \lambda_n)/2}{\lambda_m + \lambda_n} - \frac{4}{\lambda_m\lambda_n}\sin\frac{\lambda_m}{2}\sin\frac{\lambda_n}{2}\right]. \tag{46}$$

Then, with Eq. (16),

$$N_{r,m} = -\frac{\sigma T_g L}{8\varepsilon_0^2}\varepsilon_r\sum_{q=1}^{h}\varepsilon_q\sum_{n=1}^{h}U_{q,n}J_{m,n}. \tag{47}$$

2.8. Generalized mass and stiffness

The generalized mass for any symmetric eigenmode m is

$$M_m = \mu\int_{-L/2}^{L/2}\left(\cos\frac{\omega_m s}{c} - \cos\frac{\omega_m L}{2c}\right)^2\mathrm{d}s = \mu L\left[-\frac{3}{2}\frac{1}{\lambda_m}\sin\lambda_m + \frac{1}{2} + \cos^2\frac{\lambda_m}{2}\right]. \tag{48}$$

Generalized stiffness K_m may be found from M_m and the eigenfrequency of the mode. From Eq. (6) one gets

$$\lambda_m = \frac{\omega_m L}{c_g}, \quad \omega_m = \frac{c_g \lambda_m}{L} = \sqrt{\frac{K_m}{M_m}}, \quad K_m = M_m \left(\frac{c_g \lambda_m}{L}\right)^2. \tag{49}$$

2.9. Equations of motion in generalized co-ordinates

But for its non-linear term, Eq. (3) can be expressed in generalized co-ordinates for each eigenmode as

$$(M_m \omega_m^2 - K_m) u_m \cos \omega_m t = 0. \tag{50}$$

The only disturbance to this equilibrium, other than that of non-linearity, arises if the vibration frequency $r\omega_g$ differs from the eigenfrequency ω_m, and the only disturbed term is the first since only it is frequency sensitive. The disturbance amounts to

$$(r^2 \omega_g^2 - \omega_m^2) M_m u_{r,m} \cos r\omega_g t. \tag{51}$$

With manipulation this becomes

$$-\frac{\sigma T_g L}{8}\left(\frac{\lambda_m^2}{r^2} - \lambda_0^2\right) r^2 Q_m U_{r,m} \cos r\omega_g t, \tag{52}$$

in which

$$Q_m = -\frac{3}{2}\frac{1}{\lambda_m}\sin \lambda_m + \frac{1}{2} + \cos^2 \frac{\lambda_m}{2}. \tag{53}$$

The generalized forces on mode m at harmonic r, given in Eqs. (33) and (47), must balance disturbance (52). This leads to

$$-\frac{\sigma T_g L}{8}\left(\frac{\lambda_m^2}{r^2} - \lambda_0^2\right) r^2 Q_m U_{r,m} + \frac{\sigma T_g L}{8} \sum_{q=1}^{h} \left[G_{r,q} \sum_{n=1}^{h} (U_{q,n} \cdot H_{m,n}) \right] + \frac{\sigma T_g L}{8} \frac{\varepsilon_r}{\varepsilon_0} \sum_{q=1}^{h} \frac{\varepsilon_q}{\varepsilon_0} \sum_{n=1}^{h} U_{q,n} J_{m,n} = 0 \tag{54}$$

and

$$\left(\frac{\lambda_m^2}{r^2} - \lambda_0^2\right) U_{r,m} - \sum_{q=1}^{h} \sum_{n=1}^{h} \frac{G_{r,q} H_{m,n} + (\varepsilon_r \varepsilon_q / \varepsilon_0^2) J_{m,n}}{r^2 Q_m} \cdot U_{q,n}. \tag{55}$$

There is one such equation for each mode m at each harmonic r.

Now, the indices for the vectors $U_{r,m}$ and $U_{q,n}$ can be expressed as $(r-1)h + m$ and $(q-1)h + n$, respectively. Define a matrix $\mathbf{B}$ such that

$$\mathbf{B}_{(r-1)h+m,(q-1)h+n} = \frac{G_{r,q} H_{m,n} + (\varepsilon_r \varepsilon_q / \varepsilon_0^2) J_{m,n}}{r^2 Q_m}. \tag{56}$$

Then Eq. (55) can be expressed in matrix form

$$\mathrm{diag}\left(\frac{\lambda_m^2}{r^2}-\lambda_0^2\right)\cdot U_{r,m}-\mathbf{B}\cdot U_{q,n}=\mathbf{0}. \tag{57}$$

Since the first matrix is diagonal one has $U_{r,m}=U_{q,n}$, and Eq. (57) can be written as

$$\left[\mathrm{diag}\left(\frac{\lambda_n^2}{q^2}-\lambda_0^2\right)-\mathbf{B}\right]\cdot U_{q,n}=\mathbf{0} \quad \text{or} \quad \left[\mathrm{diag}\left(\frac{\lambda_m^2}{r^2}-\lambda_0^2\right)-\mathbf{B}\right]\cdot U_{r,m}=\mathbf{0} \tag{58}$$

2.10. Solution procedure

Eq. (58) is non-linear because the vector $U_{r,m}$ enters into the calculation of $\mathbf{B}$ through Eqs. (17), (22) and (34). Consequently, it cannot be solved as an eigenproblem until $U_{r,m}$ is already known or at least assumed. The procedure employed here is to assume $U_{r,m}$, calculate $\mathbf{B}$, solve Eq. (58), and then choose one of the resulting eigenvectors as the next trial $U_{r,m}$. This cycle is repeated until the solution eigenvector approaches a constant value. The process can be laborious, and this is a disadvantage of the eigenmode approach. Note that perturbation methods often permit explicit solution. On the other hand, the eigenmode approach yields benefits in terms of insights into the non-linearity mechanisms, and can permit improved accuracy in describing the mode shapes and motions at amplitudes where the perturbation parameter can no longer be considered small.

The iteration process is complicated by the fact that, at each step, the eigenanalysis produces a multitude of eigenvectors inviting exploration. If the numbers of eigenmodes and harmonics are both h, there are h^2 eigenvectors. It is evident from calculations that, at very low galloping amplitudes, h of these are associated with the linear eigenvalues λ_n, and the rest are subharmonics of them. The subharmonics are thought to be spurious. In what follows, attention is focused on the eigenmode associated with λ_1, the pseudo-fundamental, since that is the mode where non-linear effects are most pronounced.

Table 1 shows a typical set of calculation results. Note that only two independent variables enter into the calculations: δ_g and the galloping amplitude. In this table and elsewhere below, galloping amplitude is specified in terms of the amplitude/sag at midspan ($s=0$) for the

Table 1
Eigenmode amplitudes $U_{r,m}$ ($\delta_g=66$, $y_{1,1}(0)/D=0.3$)

Harmonic r	$\varepsilon_r/\varepsilon_0$	Mode m					
		1	2	3	4	5	6
1	−1.0143	**0.1624**	**−0.0266**	**−0.0326**	−0.0036	0.0000	0.0005
2	0.1785	0.0093	**0.0211**	**0.0503**	0.0043	−0.0001	−0.0009
3	−0.0361	−0.0011	0.0033	**0.0358**	−0.0058	0.0014	0.0001
4	0.0850	−0.0004	0.0007	0.0051	−0.0050	−0.0016	0.0009
5	0.0012	−0.0003	0.0002	0.0007	−0.0011	−0.0016	−0.0011
6	0.0454	−0.0001	0.0002	−0.0002	−0.0001	−0.0005	−0.0010
λ_m		7.404	10.115	15.799	22.020	28.287	34.564

fundamental harmonic of the first eigenmode, λ_1, as determined from Eq. (4), that is

$$\frac{y_{1,1}(0)}{D} = U_{1,1} \cdot \left(1 - \cos\frac{\lambda_1}{2}\right). \tag{59}$$

In Table 1, $\delta_g = 66$. The body of the table displays the normalized eigenmode amplitudes $U_{r,m}$. $\varepsilon_r/\varepsilon_0$ is shown in the second column, permitting calculation of tension variations at the various harmonics via Eqs. (16) and (24). The linear eigenvalues λ_m are displayed at the bottom. The most important components of $U_{r,m}$ are shown in bold. The fact that the components at the higher modes and higher harmonics are small indicates that six of each is quite adequate to represent the motion.

For the example of Table 1, the static tension increment was found from Eq. (40) to be $\Delta T/T_g = 0.2581$. The change in curvature $\Delta\sigma$ was then found from Eq. (41). When those changes were applied in Eq. (6), it was found that at rest $\delta_c = 46.85$.

Now, the fundamental eigenvalue that corresponds via Eq. (5) to $\delta_c = 46.85$ is $\lambda_c = 7.404$. The solution to Eq. (58) was $\lambda_0 = 7.293$. Thus, from Eq. (6),

$$\lambda_c = \frac{\omega_c L}{c_c} = 7.404, \quad \lambda_0 = \frac{\omega_g L}{c_g} = 7.293. \tag{60}$$

ω_c is the circular frequency that would be expected ignoring non-linear effects and can be calculated from at-rest conditions. ω_g is the circular frequency that actually occurs. Their specific values depend upon the physical parameters of the span, but their ratio can be determined from Eq. (60). However, it is necessary to take into account the different tensions as they enter into c_g and c_c through Eq. (6). The result turns out to be $\omega_g/\omega_c = 0.9584$.

3. Discussion

This section describes results of numerical studies utilizing the methods of the preceding section. Although the studies could not be exhaustive, it is felt that they reveal the major effects of non-linearity for the case considered: the symmetric pseudo-fundamental mode in a single "deadended" span.

3.1. Internal resonances

When the eigenfrequency of one of the higher modes is exactly twice the galloping frequency, the higher mode will respond resonantly to the generalized force (31) arising from the fundamental mode. Resonances at higher multiples of the galloping frequency may also occur. These resonances are expressed by $\lambda_n = r \cdot \lambda_0$, where r is an integer. At very low amplitudes, $\lambda_0 \approx \lambda_1$ and the resonances are easily identified by examining the ratios λ_2/λ_1, λ/λ_1, etc., as functions of δ (see Fig. 2). There turn out to be four significant resonances:

$$\lambda_2/\lambda_1 = 2 \text{ at } \delta = 16.15, \quad \lambda_3/\lambda_1 = 2 \text{ at } \delta = 85.9 \text{ and } 289, \quad \lambda_4/\lambda_1 = 3 \text{ at } \delta = 64.1.$$

The first three are evident in Fig. 3, which shows the amplitudes $U_{1,1}$, $U_{2,2}$ and $U_{2,3}$ as functions of δ_c, based on the procedures of the preceding section. Note that the absolute values are plotted. Two of the branches, identified with (−), are actually negative. While the third resonance was

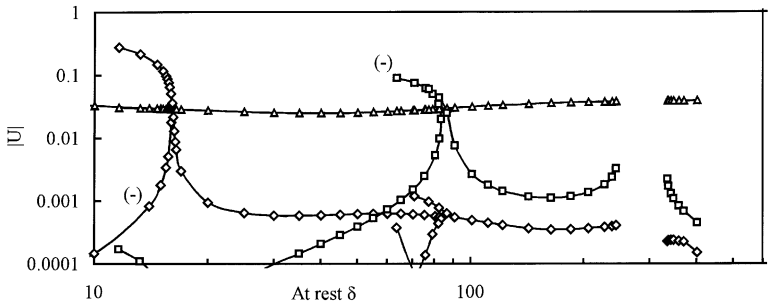

Fig. 3. Modal amplitudes for $y_{1,1}(0)/D = 0.05$. Triangles: $U_{1,1}$; diamonds: $U_{2,2}$; squares: $U_{2,3}$.

evidently present, it defied exploration. That may be due to limitations of the method or inherent instability of solutions to Eq. (58) in that δ_c range. The fourth internal resonance becomes evident only at larger galloping amplitudes.

Fig. 3 brings out two effects of non-linearity. One is a shift in the frequencies of the internal resonances as the amplitudes of the resonant modes increase. These shifts reflect a softening of the spring constants that determine the resonances. The other effect is occurrence of multiple solutions over some ranges of δ_c.

3.2. Frequency shifts

The example of Table 1 yielded a shift in the pseudo-fundamental galloping frequency of $\omega_g/\omega_c = 0.9584$. This shift actually has three components. Two are associated with the change in static tension ΔT that creates differences through Eq. (6) between δ_c and δ_g and between the wave velocities c_c and c_g. Each of δ_c and δ_g points via Eq. (5) to a set of values of λ_n, the first set pertaining to absence of non-linear effects and the second taking them into account. The fundamental roots λ_1 from each set may be used with corresponding values c_c and c_g to calculate ω_c and ω_g. However, the latter value is not quite correct. The third frequency shift component is the difference between the during-galloping value of λ_1 and λ_0. The latter is the solution to Eq. (58), and it, not λ_1, determines ω_g.

The difference between λ_0 and λ_1 during galloping deserves some comment. It arises basically from the circumstance that, were $\lambda_0 = \lambda_1$, tension variations at the second harmonic $p = 2$ would interact with curvature variations at $q = 1$ through Eq. (32) to produce a generalized force $F_{r,m}$ at harmonic $r = 1$ on the mode 1. There would be exact resonance between $F_{r,m}$ and mode 1 eigenfrequency. Infinite resonant amplification would occur. Note that the tension variations at $p = 2$ are a product of mode 1's non-linear effects. What results then is an apparent feedback loop with infinite gain. Such an absurdity in a conservative system is avoided by casting it as a multi-degree-of-freedom system interconnected with an array of (non-linear) springs. The system eigenfrequencies are then dependent variables that necessarily solve the equations of motion properly.

The magnitudes of typical frequency shift components are illustrated in Figs. 5 and 6. The figures pertain to basic galloping amplitude $y_{1,1}(0)/D = 0.3$. The most significant modal amplitudes for that case are shown in Fig. 4. Note, in that figure, that the abscissa is δ_g (during

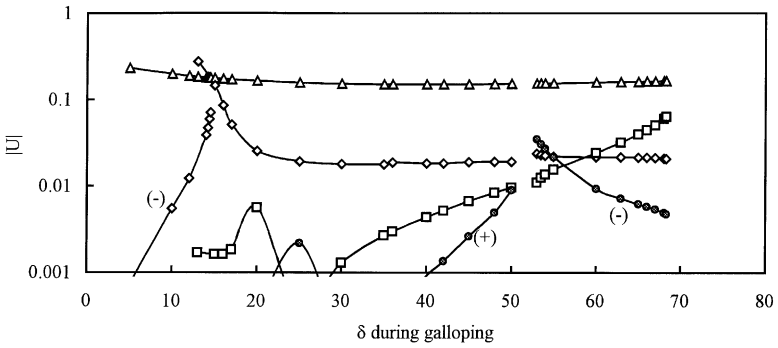

Fig. 4. Modal amplitudes for $y_{1,1}(0)/D = 0.3$. Triangles: $U_{1,1}$; diamonds: $U_{2,2}$; squares: $U_{2,3}$; circles: $U_{3,4}$.

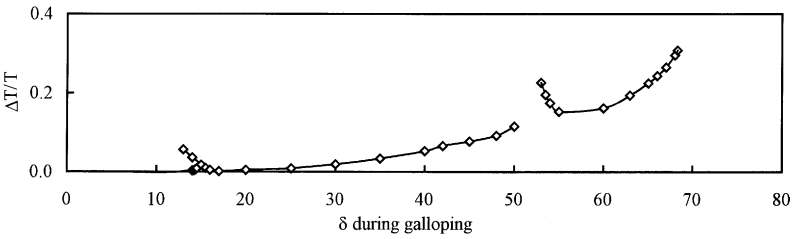

Fig. 5. Tension shifts at $y_{1,1}(0)/D = 0.3$.

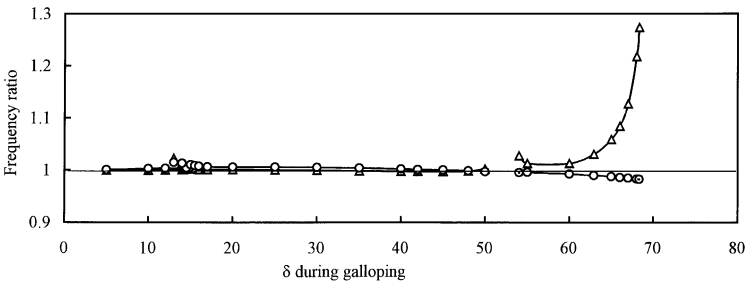

Fig. 6. Frequency shifts at $y_{1,1}(0)/D = 0.3$. Circles: λ_1/λ_c; triangles: λ_0/λ_1.

galloping) rather than at-rest δ_c as used in Fig. 3. At large amplitudes, using δ_c scrambles the curves confusingly.

The fractional shift in wave velocity is approximately half of $\Delta T/T$ shown in Fig. 5. That shift and λ_1/λ_c in Fig. 6 are caused by the change in static tension from Eq. (40), whereas λ_0/λ_1 is a purely dynamic effect of non-linearity.

3.3. Multiple solutions

Fig. 7 shows the curves for $U_{1,1}$, $U_{2,2}$ and $U_{2,3}$ from Fig. 4 plotted against at-rest δ_c. Although messy, this presentation is of interest because galloping must originate from the at-rest condition.

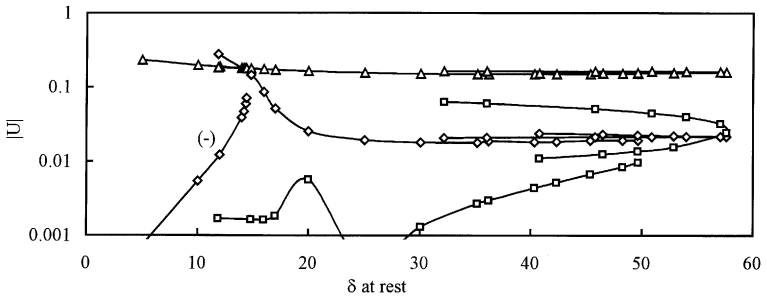

Fig. 7. Modal amplitudes for $y_{1,1}(0)/D = 0.3$ versus at-rest δ. Triangles: $U_{1,1}$; diamonds: $U_{2,2}$; squares: $U_{2,3}$.

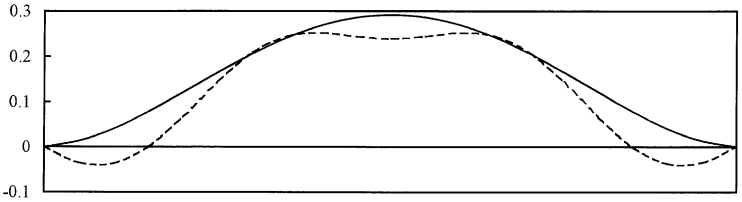

Fig. 8. Harmonic 1 mode shapes at $\delta_c = 36$ for $y_{1,1}(0)/D = 0.3$. Solid: $\delta_g = 36$; dashed: $\delta_g = 68$.

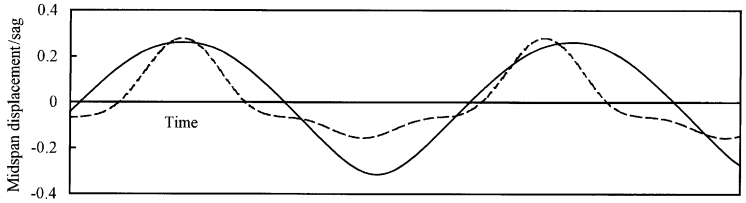

Fig. 9. Midspan waveforms for the two solutions at $\delta_c = 36$. Solid: $\delta_g = 36$; dashed: $\delta_g = 68$.

Increasing amplitude causes tension to change, and δ_g then deviates from δ_c. For the higher δ_g range, the curves double back when plotted against δ_c, presenting "upper and "lower" branches. It is evident that two different solutions are possible over a significant part of the range of δ_c. Fig. 7 brings into register the solutions that have different δ_g but originate from the same δ_c. Both solutions stem from the pseudo-fundamental linear eigenmode λ_1.

Alternative solutions at the same δ_c may have markedly different mode shapes. Fig. 8 shows the mode shape of the fundamental harmonic for the two solutions at $\delta_c = 36$. These shapes are defined by

$$Y_1(s) = \sum_{n=1}^{h} U_{1,n} \cdot \left(\cos \lambda_n \frac{s}{L} - \cos \frac{\lambda_n}{2} \right). \tag{61}$$

The shapes shown in Fig. 8 assume $Y_1(0) = 0.3$. Aerodynamic considerations would determine the actual magnitudes of these modes.

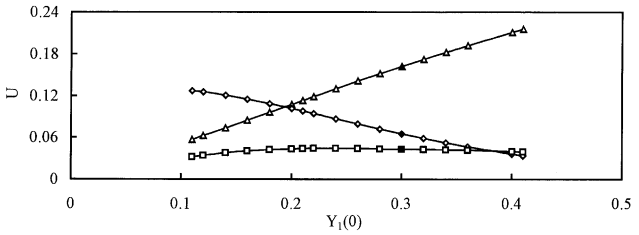

Fig. 10. Variation of modal amplitudes with galloping amplitude, $\delta_c = 36$. Triangles: $U_{1,1}$; diamonds: $U_{2,3}$; squares: $U_{3,3}$.

Alternative solutions may also have very different time-wise waveforms. For example, Fig. 9 shows midspan waveforms for the two solutions at $\delta_c = 36$, again with $Y_1(0) = 0.3$. The distortion for the upper branch $\delta_g = 68$ case is caused by significant amplitude of the $U_{2,3}$ component. The lesser fundamental amplitude results from contributions by $U_{1,2}$ and $U_{1,3}$.

These and other components change in amplitude as the galloping amplitude varies. Fig. 10 shows this variation in several components for the upper branch solution of Fig. 7 at $\delta_c = 36$. It can be seen that $U_{2,3}$ overshadows amplitude $U_{1,1}$ of the fundamental harmonic at low amplitudes, but falls to only a fraction of it at high amplitudes. Such large variations in harmonic and modal content are a feature of these upper branch solutions, and thus can occur over a significant part of the δ_c range of practical interest.

The lower solution, not shown in Fig. 10, displays negligible harmonic content at small amplitudes, growing slowly to a modest level at higher amplitudes. Only the $U_{2,2}$ component is significant. This is characteristic of lower branch solutions over much of the range of δ_c. As a general observation, the upper branch solutions are richer in modes and harmonics, Table 1 being an example.

The range of amplitudes $Y_1(0)$ covered in Fig. 10 was bounded on the high end by large tension variations leading to slackness in the cable at some point of the galloping cycle. At the low end, however, the solution procedure failed to find convergent solutions for $Y_1(0) < 0.11$. Further exploration is needed to determine whether this solution gap persists over the entire upper branch.

4. Conclusions

Non-linear effects in free symmetric-mode galloping of a shallow catenary can feasibly be addressed in the form of a non-linear eigenproblem. The motion can be represented in terms of the linear eigenmodes of the span by synthesizing the non-linear mode shape at each harmonic from the linear eigenmodes. The approach provides insight into the mechanisms involved as well as enhanced precision in representing the motions of the span. Numerical studies using the method confirm previous findings that non-linear effects cause shifts in the galloping frequency. The studies separate those shifts into tension-dependent and non-tension-dependent components. They also reveal multiple non-linear solutions for span motion for the same structural assumptions, with the different solutions marked by significant differences in mode shape and waveform.

Appendix A. Nomenclature

A cable cross-sectional area
$\mathbf{B}$ matrix of non-linear inter-harmonic and inter-modal couplings, Eq. (56)
c transverse wave velocity, Eq. (6)
D midspan sag, Eq. (11)
E elastic modulus of cable
$F_{r,m}$ generalized force from harmonic r on mode m, Eq. (27)
g gravity
G harmonic coupling parameter, Eq. (34)
H modal coupling parameter, Eq. (30)
h numbers of harmonics and eigenmodes considered
J modal coupling parameter, Eq. (46)
K generalized stiffness, Eq. (49)
L span length
m, n linear eigenmode number
M generalized mass, Eq. (48)
N generalized force due to static distortion of catenary, Eq. (44)
P distributed dynamic force due to non-linear effects, Eq. (26)
Q generalized mass parameter, Eq. (53)
p, q, r harmonic multiples of galloping frequency
S distributed static force due to non-linear effects, Eq. (37)
s spanwise location along catenary
t time
T cable tension
u eigenmode amplitude, Eq. (4)
U normalized eigenmode amplitude u/D
$U_{a,b}$ normalized amplitude of harmonic a, mode b
y local amplitude of galloping in plane of catenary
Y_1 normalized local amplitude of harmonic 1, Eq. (61)
z local displacement of cable in plane of catenary
δ catenary elasticity parameter, Eq. (6)
ε a component of cable strain, Eqs. (12) and (18)
ε_0 static component of cable strain, Eq. (16)
ζ dynamic component of tension
λ eigenvalue of linear galloping mode, Eq. (6)
τ amplitude of dynamic component of tension
μ cable unit mass
σ curvature of catenary
φ eigenmode shape, Eq. (28)
ω circular frequency

Subscripts
c cable at rest
g cable galloping

References

[1] K.A. Foss, Methods for computing the mechanical dynamic response of electric power transmission lines, Progress Report No. 4, Research Study on Galloping of Electric Power Transmission Lines, Aeroelastic and Structures Research Laboratory, MIT, Cambridge, MA, August 1, 1960.
[2] A.I. Soler, Dynamic response of single cables with initial sag, *Journal of the Franklin Institute* 290 (4) (1970) 377–387.
[3] H.M. Irvine, T.K. Caughey, The linear theory of free vibrations of a suspended cable, *Proceedings of the Royal Society of London A* 341 (1974) 299–315.
[4] C.B. Rawlins, Galloping eigenmodes in a multispan overhead line section, *Proceedings of the Fourth International Symposium on Cable Dynamics*, Montreal, Canada, 2001, pp. 85–92.
[5] J.P. Den Hartog, Transmission line vibration due to sleet, *AIEE Transactions* 51 (Part 4) (1932) 1074–1086.
[6] P. Yu, Y.M. Desai, A.H. Shah, N. Popplewell, Three-degree-of-freedom model for galloping, *Journal of Engineering Mechanics* 119 (12) (1993) 2404–2448.
[7] D.G. Havard, Dynamic loads on transmission line structures during galloping, *Proceedings, IWAIS 2002*, Brno, Czech Republic, 2002.
[8] P. Hagedorn, B. Schäfer, On nonlinear free vibrations of an elastic cable, *International Journal of Nonlinear Mechanics* 15 (1980) 333–340.
[9] A. Luongo, G. Rega, F. Vestroni, Monofrequent oscillations of a non-linear model of a suspended cable, *Journal of Sound and Vibration* 82 (2) (1982) 247–259.
[10] S.W. Rienstra, A nonlinear theory of free vibrations of single and coupled suspended elastic cables, Report IWDE 88-06, Instituut Wiskundige Dienstverlening Eindhoven, July 1988.